Molecular-scale remnants of the liquid-gas transition in supercritical polar fluids

V. P. Sokhan,[1] A. Jones,[2] F. S. Cipcigan,[1,2] J. Crain,[1,2] and G. J. Martyna[3]

[1]*National Physical Laboratory, Hampton Road, Teddington, Middlesex TW11 0LW, UK*

[2]*School of Physics and Astronomy, The University of Edinburgh, Mayfield Road, Edinburgh EH9 3JZ, UK*

[3]*IBM T. J. Watson Research Center, Yorktown Heights, New York 10598, USA*

(Dated: August 6, 2015)

Abstract

An electronically coarse-grained model for water reveals a persistent vestige of the liquid-gas transition deep into the supercritical region. A crossover in the density dependence of the molecular dipole arises from the onset of non-percolating hydrogen bonds. The crossover points coincide with the Widom line in the scaling region but extend further, tracking the heat capacity maxima, offering evidence for liquid- and gas-like state points in a one-phase fluid. The effect is present even in dipole-limit models suggesting that it is common for all molecular liquids exhibiting dipole enhancement in the liquid phase.

PACS numbers: 31.15.-p, 31.15.xk, 61.20.Ja, 61.25.Em, 64.60.F-, 65.20.Jk

There is a distinct boundary between liquid and vapor phases of a substance separated by a coexistence line over a finite range of pressures (p) and temperatures (T). Crossing the line results in a discontinuous density change – the hallmark of a first-order phase transition. The coexistence line terminates at a critical point in the (T, p) plane beyond which the thermodynamic distinction between liquid and gas phases is lost and a single-phase supercritical fluid is formed. In this region, there are no further phase boundaries and the supercritical fluid permits a continuous path from liquid to gas over a broad range of thermodynamic states [1]. In water, for example, this tunability can be exploited to control solvation properties making supercritical water an important ingredient in industrial processes and a promising "green" alternative to chemical solvents [2–4].

While the classical thermodynamic picture is well understood, the molecular nature of supercritical fluids remains a largely open question. Key issues for water are (1) structure and hydrogen bonding (HB) in the supercritical region; (2) the electronic redistribution which occurs in the water molecules as the HB network is reconfigured; and (3) most broadly, the relationship of the supercritical fluid to fundamental liquid and gaseous states of matter that exist as separate phases below T_c.

In this context, the observation that certain thermophysical response functions exhibit maxima in the transition region between gas-like and liquid-like states of the supercritical phase has prompted the suggestion that a remnant of coexistence may extend into the supercritical region [5]. The locus of such maxima is referred to as the Widom line [6]. Direct confirmation of distinct gas-like and liquid-like state points, however, is lacking though some evidence of dynamical crossover phenomena has been reported in noble gases [5, 7]. Analogous concepts may apply at low temperatures where a Widom line is proposed to extend from a hidden liquid-liquid critical point [6] influencing the properties of supercooled water.

Supercritical water poses unique challenges for molecular models because conventional empirical interaction potentials capture neither the electronic redistribution which occurs along an isotherm within the supercritical region of the phase diagram (dipole, quadrupole and higher manybody polarization responses) nor the manybody dispersion forces which have emerged as an important aspect of water physics [8, 9]. Moreover, as these empirical models are typically optimized to describe liquid water near ambient conditions, their transferability to the supercritical fluid is questionable and the resulting physical insight into the molecular processes which occur above the critical point is limited.

A new approach for materials simulation has been proposed recently wherein the molecular

electronic distribution is not represented by a parametrized mean-field model, but rather by a coarse-grained description based on embedded harmonic oscillators – the quantum Drude oscillator (QDO) model [10, 11]. As the oscillators are treated quantum mechanically, this model generates the complete hierarchy of many-body polarisation and dispersion phenomena which when solved in strong coupling, as here, ensures that all potential symmetry-breaking interactions are present within Gaussian statistics. The responses (to all orders) include, but are not limited to, inductive responses leading to distortions of the electronic charge distribution and to van der Waals and higher-order dispersion interactions arising from quantum mechanical charge density fluctuations. The model parameters are fit to leading-order responses of the isolated molecule providing a perfect low-density limit [9, 12, 13]. Here we apply the model with the short-range repulsion parameterized to a high-level ab initio calculations of the water dimer, (see Refs [9, 14] for model details).

In prior work [9], using the methodology described in [10–13] to simulate the model, we have determined the location of its critical point as $\{T_\mathrm{c} = 649(2)$ K, $\rho_\mathrm{c} = 0.317(5)$ g/cm$^3\}$, which is in accord with experiment $\{T_\mathrm{c} = 647.096$ K, $\rho_\mathrm{c} = 0.322$ g/cm$^3\}$ [15]. The dielectric properties along coexistence as well as the orthobaric densities of both the gas and liquid branches are well described [9]. We regard the prediction of an accurate critical point as a prerequisite for reliable examination of the supercritical phase. We are aware of no other description able to predict an accurate critical point from the properties of the isolated molecule.

Having established the critical point and the dielectric properties of the model, we are now in position to examine the molecular properties across several supercritical isotherms and to draw broader conclusions about the molecular nature of supercritical water. To set the context for this part of the work, we draw attention to recent studies which have explored the extent to which the notion of liquid-gas coexistence can be extended past the critical point. Typically, this extrapolation is based on identifying the loci of maxima in second-order thermodynamic response functions such as heat capacity (C_p), thermal expansivity (α) or isothermal compressibility (κ_T) along isothermal paths. In atomic systems (noble gases), evidence of dynamic anomalies near the points of maxima in C_p has been reported [7] and interpreted as a signature of liquid- and gas-like behavior. However, it is clear that the extrema of different thermodynamic functions rapidly diverge from each other above the critical point and only collapse onto a universal Widom line in the asymptotic scaling region near the critical point as described by a scaling theory developed in Ref. [1]. Beyond this region, and further into the one-phase supercritical field, it is unclear whether

any specific thermodynamic observable separates distinct regimes which can be unambiguously associated with liquid- or gas-like behavior.

We now consider the dipole moment of water as a local reporter of molecular environment. Individual water molecules which are adaptive and responsive to their environment, become strongly polarized as a result of the highly directional bonding of the liquid-like state [16]. We explored the supercritical region along several isotherms from 673 K to 1083 K and for densities from 2 mol/l to 60 mol/l spanning from 10 MPa to 2.4 GPa. The results of our calculations of the molecular dipole at two isotherms in the supercritical region of the phase diagram are shown in Fig. 1. The dipole's density dependence exhibits a change in slope at $\rho = 17.1$ mol/l at 673 K and 18.9 mol/l at 873 K. The corresponding densities of heat capacity maxima, obtained from the IAPWS-95 reference equation of state for water [15], are 17.25 mol/l and 18.91 mol/l. The dipole crossover is still detectable at $T = 1083\,\mathrm{K} = 1.7 \times T_c$ above which it disappears in statistical noise. It becomes more pronounced with decreasing temperature and below T_c it occurs in the two-phase region.

In order to investigate further the crossover in the dipole moment we analyze another microscopic discriminator between the liquid-like and gas-like states – hydrogen bonding (HB). Although the presence of a HB network in the supercritical region is well established by various techniques [17–19], the structure and the topology of the network in liquid water is a matter of discussion [19–22]. Examining HB connectivity, we find that local tetrahedral order persists down to low gas-like densities at supercritical temperatures. Using the distance-angle geometric definition of the hydrogen bond of Ref. [23] we observe a similar, albeit less pronounced, crossover in density dependence of the average number of hydrogen bonds per molecule, which occurs at the same densities as the crossover in dipole moment, shown in Fig. 1.

The number of hydrogen bonds per molecule at 673 K and density $\rho = 30$ mol/l (0.54 g/cm^3) is 40% of that of ambient water, 300 K, 55.32 mol/l, where $n_{\mathrm{HB}} = 3.71$. This can be compared with 29% of ambient at the same temperature and 28.9 mol/l estimated from NMR chemical shift measurements [17]. The number of hydrogen bonds per molecule at the crossover density, which decreases slightly from 1.08 at $T = 673$ K to 0.85 at $T = 1083$ K, is well below the percolation threshold which occurs at $n_{\mathrm{HB}} = 1.53(5)$ according to Ref. [24]. This observation is in accord with Raman experiments [22], which are interpreted to indicate no tetrahedral hydrogen bonding at the critical point. We note that collective properties which may show dynamic or viscoelastic anomalies may also be detectable by x-ray scattering techniques or other experimental probes of relaxation processes. We therefore conclude that the onset of the formation of minimal

HB associations corresponds to the dipole crossover point in the supercritical field which, with decreasing temperatures, evolves to the liquid-gas coexistence line in the two phase region.

The results of the study are summarized in Fig. 2, where we plot the positions of the observed crossover points in the (T, p) plane along with the portion of the coexistence line ending in the critical point and experimental data showing maxima in various response functions. Shown here are specific heat, C_p, isothermal compressibility, κ_T, and thermal expansivity, α. Asymptotically close to the critical point, in the region $T_{\rm c} < T < T_{\rm W}$, the dipole crossover points occur along the Widom line, where the loci of all response function maxima coincide. Moreover, the dipole values are unambiguously vapor-like on the low-p side and liquid-like on the high-p side. On the molecular scale it therefore appears possible to partially extend the notion of coexistence and the liquid–gas transition well into the thermodynamically single-phase fluid as a remnant.

At higher temperatures, in the non-asymptotic region $T_{\rm W} < T < T_{\rm H}$, the loci of response function maxima diverge from the Widom line but it appears that the dipole crossover most closely tracks $C_p(T)$. Above $T_{\rm H}$ the dipole derivative transition becomes undetectable and fluid appears homogeneous at all lenthscales. We note that the formation of HB dimers creates an additional thermal reservoir which contributes to the specific heat in liquid water. We therefore speculate that this may be the molecular origin of the close link revealed here between dipole-crossover, hydrogen bond formation, remnant liquid-gas coexistence behavior in the supercritical phase and the locus of maxima in C_p in and beyond the scaling region. No such direct link exists between HB formation and thermal expansivity or isothermal compressibility the maxima of which follow very different trajectories out of the scaling region.

Finally, we examine the structure and density at several thermodynamic state points for which experimental data are available [25]. We focus first on the $T = 673$ K isotherm and compare the results to neutron diffraction measurements [25]. Predicted densities along this isotherm are shown in Fig. 3 together with data obtained from IAPWS-95 reference equation of state [15]. Since our QDO model does not involve any condensed-phase parameterisation, the agreement arises as a prediction and gives confidence in the previously presented results.

Further structural data is presented in the insets to Fig. 3, which show three-dimensional first coordination shell plots for oxygen (red) and hydrogen (white) of surrounding water molecules. The isosurfaces are drawn at $2\times$ (bulk density) levels. These illustrate the extent of hydrogen bond reconfiguration which occurs at various densities along the isotherm. The partial radial distribution functions are shown in Fig. 4 for $T = 673$ K, $p = 340$ MPa (red lines) in comparison to the neutron

diffraction data of Ref. [25] (blue lines). Subtle features of the experimental H–H distributions are present in the model, and the O–O correlations are captured as well.

In Fig. 1, the mean molecular dipole moment $|\bar{\mu}|$ is seen to vary linearly with density in two regions, which can be understood using the following argument: The induced dipole moment is proportional to the local field acting on a water molecule, which can be decomposed into contributions from the first coordination shell and from the rest of the fluid. As ab initio and induction model calculations of small water clusters [26] have shown, the water dipole moment scales linearly with the cluster size for up to five members in the cluster. A mean field estimate assuming the average distance to scale like $\rho^{-1/3}$ leads to the same conclusion. More deeply, the Onsager reaction field strength scales linearly with density [27].

For strongly associated liquids like water, the Widom line has been connected with a percolation transition in the hydrogen-bond network [28]. However, our results support the view that the origin of the crossover and the extrema in the response functions is more local. We show that this behavior extends much further into the notionally one-phase region and can be detected as far as $T = 1.7 \times T_{\rm c}$ tracking most closely the maxima in the specific heat. Only along the isotherms beyond these temperatures does it appear that supercritical water is a homogeneous fluid on the molecular scale exhibiting no detectable remnants of the liquid-gas transition. The extent of hydrogen bonding across the Widom line and beyond the scaling region can, in principle, be indirectly accessed by Raman scattering measurements of the OH stretch band which is a reporter of hydrogen bonding and the integrity of the network. Collective properties which may show dynamic or viscoelastic anomalies may also be detectable by x-ray scattering techniques or other experimental probes of relaxation processes.

In order to address the question of generality of the phenomena reported here we studied two dipole polarizable models (polarization treated in the electric dipole limit), namely the classical Drude oscillator model, SWM4-NDP [29], for which the critical parameters are known [30]: $T_{\rm c}^{\rm dip} = 0.89T_{\rm c}$, $p_{\rm c}^{\rm dip} = 0.90p_{\rm c}$, $\rho_{\rm c}^{\rm dip} = 1.02\rho_{\rm c}$, in terms of experimental values for water. The second is a polarizable version of the Stockmayer model, the 'minimalist' (purely dipolar) fluid model with a different local association topology [31], and estimated critical parameters $T_{\rm c}^{\rm s} = 1.1T_{\rm c}$, $p_{\rm c}^{\rm s} = 1.5p_{\rm c}$, $\rho_{\rm c}^{\rm s} = 1.02\rho_{\rm c}$ (see Ref. [14]). Finite size effects are investigated and ruled out in Supplementary Material [14]. The results for three models, presented in Fig. 5, show that the dipole moment change is most pronounced in fully responsive QDO, but also emerges from dipole-polarizable water model and the polarizable Stockmayer model. The reduced crossover density for

QDO model $\rho_{\times}^{*} = 0.90$, and shifts to 0.63 for SWM4-NDP and to 0.56 for the Stockmayer model. Therefore, our study has revealed an intriguing new property of associating liquids, the extension of gas-liquid critical effects on the molecular dipole moment.

In summary, we find direct evidence of molecular-scale heterogeneity in supercritical polar fluids. A clearly identifiable transition between dissociated (gas like) and associated (liquid like) regimes is evidenced by a change in the density dependence of the molecular dipole moment accompanied by a transition in the hydrogen bond connectivity. This characteristic signature has been observed in a fully responsive electronic model of water which provides an excellent prediction of the ambient, critical and supercritical properties but is also present in simpler dipole-limit models with two different association topologies – the minimal model class in which the the behavior may be observed. While the simpler models do not predict the critical point accurately for water they nevertheless provide compelling evidence that the phenomenon is likely to be general for polar liquids. The observations provide a molecular basis for the variety of response function anomalies which define the "Widom line" asymptotically close to the critical point. This is also significant outside the scaling regime where the maxima of thermodynamic response functions follow different trajectories making it unclear which, if any, separate liquid-like from gas-like regions. Here we observe that the dipole crossover points follow only the heat capacity maximum outside of the scaling region and their correlation to rudimentary hydrogen bonding establishes an unambiguous extension of the liquid-gas coexistence line deep into the supercritical phase.

This work was supported by the NPL Strategic Research programme, the Engineering and Physical Sciences Research Council (EPSRC) and the European Metrology Research Programme (EMRP). Generous allocation of time on BG/Q at STFC Hartee Centre, UK, is gratefully acknowledged.

[1] H. E. Stanley, *Introduction to Phase Transitions and Critical Phenomena* (Oxford University Press, New York, 1971).

[2] Y. Arai, T. Sako, and Y. Takebayashi, eds., *Supercritical Fluids* (Springer, Berlin–Heidelberg, 2002).

[3] N. Akiya and P. E. Savage, Chem. Rev. **102**, 2725 (2002).

[4] C. A. Eckert, B. L. Knutson, and P. G. Debenedetti, Nature **383**, 313 (1996).

[5] V. V. Brazhkin, Y. D. Fomin, A. G. Lyapin, V. N. Ryzhov, and E. N. Tsiok, J. Phys. Chem. B **115**,

14112 (2011).

[6] L. Xu, P. Kumar, S. V. Buldyrev, S.-H. Chen, P. H. Poole, F. Sciortino, and H. E. Stanley, Proc. Natl Acad. Sci. USA **102**, 16558 (2005).

[7] G. G. Simeoni, T. Bryk, F. A. Gorelli, M. Krisch, G. Ruocco, M. Santoro, and T. Scopigno, Nat. Phys. **6**, 503 (2010).

[8] M. J. Gillan, D. Alfè, A. P. Bartók, and G. Csányi, J. Chem. Phys. **139**, 244504 (2013).

[9] V. P. Sokhan, A. Jones, J. Crain, F. Cipcigan, and G. Martyna, Proc. Natl Acad. Sci. USA **112**, 6341 (2015).

[10] T. W. Whitfield and G. J. Martyna, Chem. Phys. Lett. **424**, 409 (2006).

[11] T. W. Whitfield and G. J. Martyna, J. Chem. Phys. **126**, 074104 (2007).

[12] A. P. Jones, J. Crain, V. P. Sokhan, T. W. Whitfield, and G. J. Martyna, Phys. Rev. B **87**, 144103 (2013).

[13] A. Jones, F. Cipcigan, V. P. Sokhan, J. Crain, and G. J. Martyna, Phys. Rev. Lett. **110**, 227801 (2013).

[14] (2015), see Supplemental Material at [*URL will be inserted by publisher*] for the Drude model parameters and simulation details.

[15] W. Wagner and A. Pruß, J. Phys. Chem. Ref. Data **31**, 387 (2002).

[16] J. D. Bernal and R. H. Fowler, J. Chem. Phys. **1**, 515 (1933).

[17] M. M. Hoffmann and M. S. Conradi, J. Am. Chem. Soc. **119**, 3811 (1997).

[18] P. Wernet, D. Testemale, J.-L. Hazemann, R. Argoud, P. Glatzel, L. G. M. Pettersson, A. Nilsson, and U. Bergmann, J. Chem. Phys. **123**, 154503 (2005).

[19] M. Bernabei, A. Botti, F. Bruni, M. A. Ricci, and A. K. Soper, Phys. Rev. E **78**, 021505 (2008).

[20] P. Wernet, D. Nordlund, U. Bergmann, M. Cavalleri, M. Odelius, H. Ogasawara, L. Å. Näslund, T. K. Hirsch, L. Ojamäe, P. Glatzel, L. G. M. Pettersson, and A. Nilsson, Science **304**, 995 (2004).

[21] T. Head-Gordon and M. E. Johnson, Proc. Natl Acad. Sci. USA **103**, 7973 (2006).

[22] Q. Sun, Q. Wang, and D. Ding, J. Phys. Chem. B **118**, 11253 (2014).

[23] R. Kumar, J. R. Schmidt, and J. L. Skinner, J. Chem. Phys. **126**, 204107 (2007).

[24] R. L. Blumberg, H. E. Stanley, A. Geiger, and P. Mausbach, J. Chem. Phys. **80**, 5230 (1984).

[25] A. K. Soper, Chem. Phys. **258**, 121 (2000).

[26] J. K. Gregory, D. C. Clary, K. Liu, M. G. Brown, and R. J. Saykally, Science **275**, 814 (1997).

[27] L. Onsager, J. Am. Chem. Soc. **58**, 1486 (1936).

[28] L. B. Partay, P. Jedlovszky, I. Brovchenko, and A. Oleinikova, J. Phys. Chem. B **111**, 7603 (2007).

[29] G. Lamoureux, E. Harder, I. V. Vorobyov, B. Roux, and A. D. M. Jr., Chem. Phys. Lett. **418**, 245 (2006).

[30] P. T. Kiss and A. Baranyai, J. Chem. Phys. **137**, 194103 (2012).

[31] M. van Leeuwen, Fluid Phase Equilibria **99**, 1 (1994).

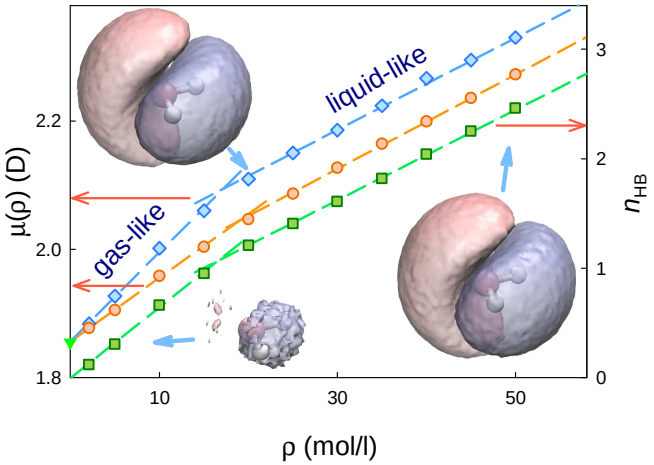

FIG. 1. (Color online). Average molecular dipole moment as a function of density at $T = 673$ K, blue diamonds, and at $T = 873$ K, orange circles. The triangle denotes the isolated monomer value (parameter of the model). Green squares and right scale, average number of hydrogen bonds per molecule as a function of density at $T = 673$ K. The lines are the linear fits to data. Insets illustrate the variation in electron density with pressure, where the pink and blue isosurfaces correspond to gain and loss of the electron density.

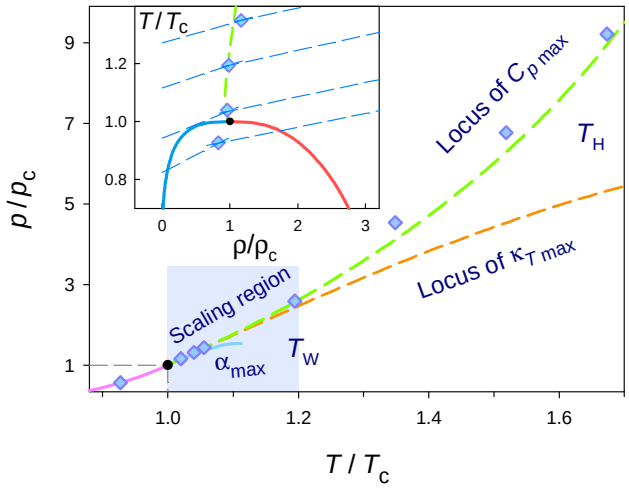

FIG. 2. (Color online). (T, p) phase diagram of water in the proximity of the critical point in units of critical temperature, T_c, and critical pressure, p_c. The liquid-vapor coexistence curve (pink), the loci of maxima in heat capacity (green), thermal expansivity (orange), and isothermal compressibility (blue), obtained using the IAPWS-95 reference EOS [15]. The blue diamonds represent our results derived from the analysis of Fig. 1. The black dot marks the critical point. The inset, the corresponding (ρ, T) phase diagram in reduced units, shows the gas and liquid branches of the coexistence curve, the locus of the heat capacity maxima, and superimposed are linear fits to the dipole moment (the blue dashed lines) in gas- and liquid-like regions with vertical offsets to map the corresponding temperatures at the crossover. The crossover densities are denoted by the diamonds. The scaling theory of Ref. [1] predicts the "true Widom line" for water where $\partial p/\partial T > 0$ follows κ_T.

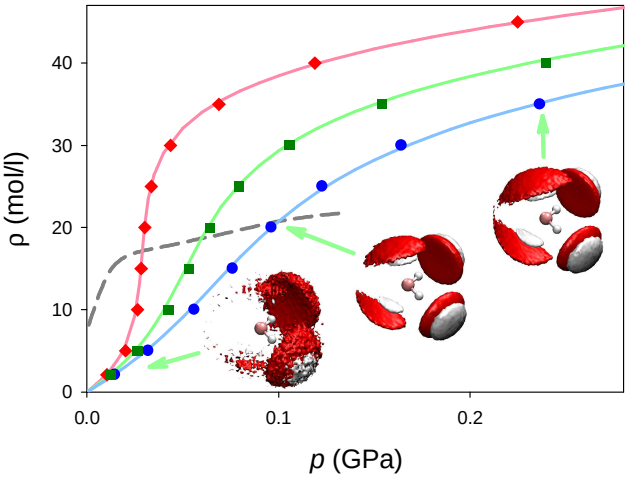

FIG. 3. (Color online). Density of water along the $T = 673$ K, 773 K, and 873 K isotherms (from top to bottom) as obtained in APIMD-QDO simulation (symbols) vs experimental data(full lines). All simulated states, apart from the first four in each isotherm, are in the conventional supercritical region [2]. The dashed line indicates the crossover densities. Insets, the 3D plots showing first oxygen (red) and hydrogen (white) coordination shells, illustrate remarkable persistence of tetrahedral structure at $T = 673$ K.

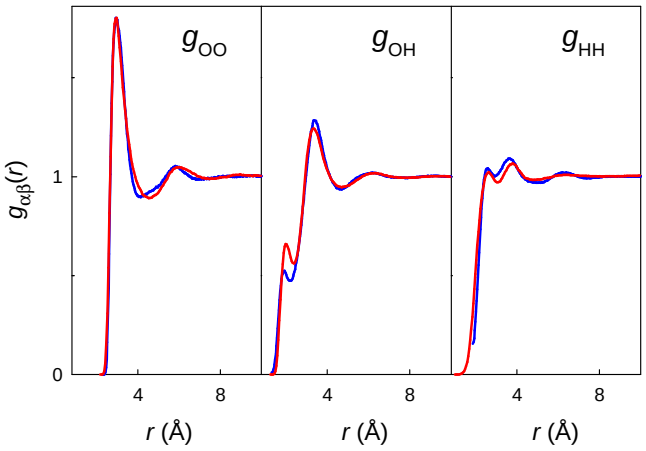

FIG. 4. (Color online). The partial radial distribution functions obtained in the QDO water model simulation under supercritical conditions at $T = 673$ K and $p = 340$ MPa (red lines). Also shown for comparison are distribution functions obtained from neutron scattering [25] at the same thermodynamic conditions (blue lines).

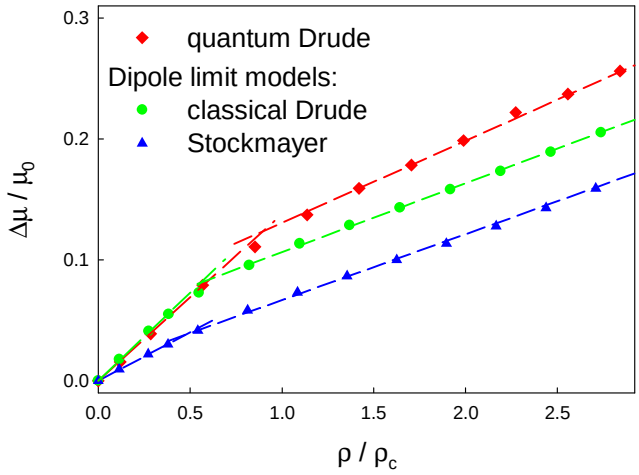

FIG. 5. (Color online). Relative (to the gas-phase value) enhancement of the molecular dipole moment as a function of the reduced density. Red diamonds, quantum Drude model; green circles, classical Drude oscillator model (dipole limit); blue triangles, polarizable Stockmayer model (dipole limit). All calculations were performed at a reduced temperature $T^* = 1.036\,T_\mathrm{c}$ in terms of corresponding critical temperature T_c. Straight lines are to guide the eye.

Supplemental Material:

Molecular-scale signatures of the liquid-gas transition observed in supercritical water

V. P. Sokhan,[1] A. Jones,[2] F. S. Cipcigan,[1,2] J. Crain,[1,2] and G. J. Martyna[3]

[1]*National Physical Laboratory, Hampton Road, Teddington, Middlesex TW11 0LW, UK*
[2]*School of Physics and Astronomy, The University of Edinburgh, Mayfield Road, Edinburgh EH9 3JZ, UK*
[3]*IBM T. J. Watson Research Center, Yorktown Heights, New York 10598, USA*

The layout

A description of the model and simulation methods are provided first. Second, the hydrogen bond definition employed in the text is described and justified. A mean-field treatment of the scaling of molecular moment with density is given next. The Stockmayer model is described next followed by a discussion of finite size effects. Last, we address the different local association topology of water models and the Stockmayer fluid.

The model and simulation details

For water, which has nearly isotropic polarizability, we follow the model construction reported in Ref. [1]. The quantum Drude oscillator (QDO) model for water, sketched in Fig. 1, is based on rigid TIP4P geometry of the monomer ($r_{\rm OH} = 95.72$ pm, $\angle$HOH $= 104.52^\circ$). A *drudon* (quantum Drude oscillator) is tethered to a point M along the $\angle$HOH bisector at a distance $r_{\rm OM} = 26.67$ pm from the oxygen nucleus. The model parameters are chosen such that the long-range responses match reference values of the monomer and dimer (gas-phase polarizabilities and pair-dispersion coefficients). Three fixed point charges, two on hydrogens, $q_{\rm H} = 0.605|e|$, and one on M–point, $q_{\rm M} = -2q_{\rm H}$, are taken to represent the isolated molecule limit, matched to the low order electrostatic moments. The drudon is also tethered to M–point. Its parameters in atomic units are: mass, $m_{\rm D} = 0.3656\, m_e$, charge, $q_{\rm D} = -1.1973|e|$, and angular frequency, $\omega = 0.6287\, E_h/\hbar$.

The Coulomb forces are regularized at short range by assigning small Gaussian widths to the charges, $\sigma_{\rm H} = \sigma_{\rm D} = 0.1a_0$, and $\sigma_{\rm C} = 1.2a_0$ for the QDO center. To correct for missing in the QDO model Fermion exchange a biexponential term

$$\phi(r) = \kappa_1 \exp(-\lambda_1 r) + \kappa_2 \exp(-\lambda_2 r)$$

has been added between oxygens, providing the required repulsion. The parameters $\kappa = \{613.3, 10.5693\}$

and $\lambda = \{2.3244, 1.5145\}$ were obtained from a fit to the difference between a reference quantum chemical dimer ground state potential energy surface (CCSD(T)-level) and that of the QDO's, calculated using norm-conserving diffusion Monte Carlo [2]. In order to reproduce accurately the equation of state fully convergent ab initio calculations required for the reference potential surface. In Mark I model we fit to empirical potential [1], which effectively included manybody interactions, and as a result, the experimental density was reproduced when dispersion interactions were scaled up by 37%.

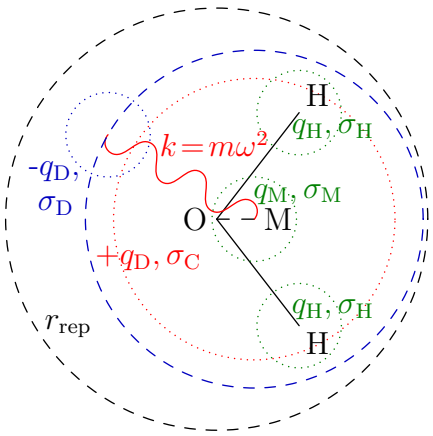

FIG. 1: QDO model for water.

The system is thus defined by monomers with "perfect" (by construction) long-range electrostatics and all resulting condensed phase behavior emerges as a model prediction. No additional thermodynamic data or liquid state information was used.

The coarse grained Hamiltonian for the quantum Drude oscillator (QDO) water model is

$$H = \sum_i T_i^{(\mathrm{rig})} + \phi^{(\mathrm{Coul})}(\mathbf{R}) + \sum_{j \neq i} \phi^{(\mathrm{rep})}\left(R_{\mathrm{O}ij}\right) + E_0^{(\mathrm{D})}(\mathbf{R}),$$

$$\hat{\mathbf{H}}^{(\mathrm{D})} \psi_0(\mathbf{r}, \mathbf{R}) = E_0^{(\mathrm{D})}(\mathbf{R})\, \psi_0(\mathbf{r}, \mathbf{R}),$$

$$\hat{\mathbf{H}}^{(\mathrm{D})} = \sum_i \left(\hat{\mathbf{T}}_i + \frac{\mu\omega^2}{2} (\mathbf{r}_i - \mathbf{R}_{\mathrm{c}i})^2 \right) + \phi^{(\mathrm{Coul})}(\mathbf{r}, \mathbf{R}).$$

Here, $T_i^{(\mathrm{rig})}$ is the classical rigid body kinetic energy of water molecule i; $9N$-vector $\mathbf{R}$ represents the coordinates of all the water molecules in the system; $\phi^{(\mathrm{Coul})}(\mathbf{R})$ is the intermolecular Coulomb interaction energy between the fixed monomer gas phase charge distributions only; $\phi^{(\mathrm{rep})}\left(R_{\mathrm{O}ij}\right)$ is an oxygen-centered pair-wise repulsion. The quantities $E_0^{(\mathrm{D})}(\mathbf{R})$ and $\psi_0(\mathbf{r}, \mathbf{R})$ are the ground state Born–Oppenheimer energy surface and wavefunction of the QDO electronic structure, respectively; $\mathbf{r}_i$ and $\hat{\mathbf{T}}_i$ are the position and quantum kinetic energy of the oscillator centered on molecule i. The oscillators centered at $\mathbf{R}_{\mathrm{c}i}$ are characterized

by parameters $\{\mu, \omega, q\}$. Finally, $\phi^{(\mathrm{Coul})}(\mathbf{r}, \mathbf{R})$ is intermolecular Coulomb interaction between the Drude particles of charge q^-, at position $\mathbf{r}$, their center of oscillation with charge q^+, at position $\mathbf{R}_\mathrm{c}$, and the fixed monomer charge distribution. Regularization of the Coulomb interaction is discussed elsewhere [3].

Finite temperature condensed phase calculations were performed using adiabatic path integral molecular dynamics for quantum Drude oscillators (APIMD-QDO) [4–6] in the canonical and isothermal-isobaric ensembles [7]. We used the discretized (high-temperature) path integral approximation to the partition function with the number of beads (the Trotter number) $P = 96$ and adiabaticity factor $\gamma = 16$ and close to Widom line densities, $\gamma = 32$.

All calculations were performed for canonical (NVT) or isothermal-isobaric (NpT) conditions using cubic systems containing 300 water molecules with 3D periodic boundary conditions and Ewald summation technique for electrostatic interactions. At 673 K we recalculated all density points with $N = 1000$ molecules and the results were statistically identical to that smaller system. This is the consequence of the absence of any truncation scheme in intermolecular interactions and of the short range of structural and orientational ordering at high temperatures. The integration timestep for adiabaticity factor $\gamma = 16$ was $dt = 0.15$ fs ($6.25\,\hbar/E_h$) and a typical integration time was 150 ps ($10^6 dt$), which requires ca. 27 h of CPU time on BlueGene/Q running on 8K cores.

Finite size effects estimation

In order to verify that our results converged with respect to integration time and system size, for one thermodynamic point, $T^* = 1.036$ and density $\rho^* = 0.82$ we performed a set of test calculations using SWM4-NDP model for systems with $N = 300$, 1,000, 4,000, 12,500, and 100,000 molecules. The Drude oscillator degrees of freedom were treated as dynamic variabled and extended Lagrangian equations of motion were integrated with 0.5 fs timestep, and the temperature was controlled by two thermostats with classical Drude oscillators kept close to 1 K by Langevin thermostat. The obtained results for the dipole moment convergence are shown in Fig. 2. They fit well to $1/N$ (shown in the Figure by the dashed line) and from this fit the dipole moment extrapolated to infinite size is only than 0.1% higher than the value obtained with the smallest studied system. No systematic drift in statistical properties has been observed after equilibrating the systems for at least 200 ps.

Special care was taken to ensure that there are no systematic drift in computer properties, for which long runs, from 0.1 μs for $N = 300$ to 1 ns for $N = 10^5$ have been performed. In all cases pressure was $p = 24.81(4)$ MPa.

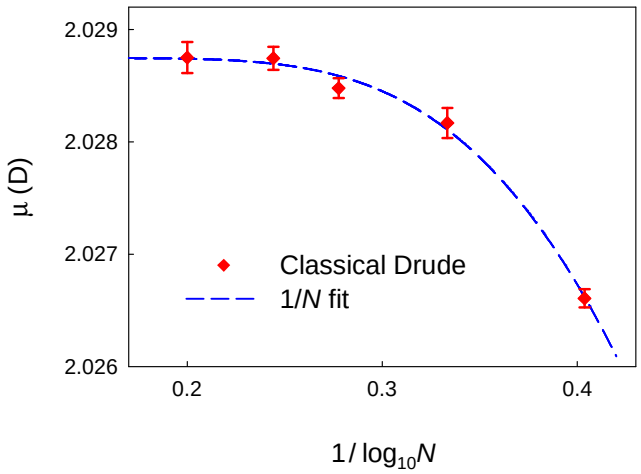

FIG. 2: System size dependence of the molecular dipole moment calculated for the classical Drude model at reduced density $\rho^* = 0.82$ and reduced temperature $T^* = 1.036$. The error bars correspond to two standard deviations (95% confidence level).

Hydrogen bonding

When calculating various HB distributions we used the geometric $R - \beta$ distance-angle definition of the hydrogen bond [8], in which two water molecules are considered hydrogen-bonded if and only if the O–O distance between two molecules is shorter than the certain threshold value, R_{HB}, and the angle β between O–H bond and the candidate molecule oxygen, $\mathrm{O-H\cdots O}$, is smaller than the specified criterion β_{HB}. We have found that the values $R_{\mathrm{HB}} = 3.5$ Å and $\beta_{\mathrm{HB}} = 30^\circ$ are suitable for the studied cases (see Fig. 3).

Molecular moment scaling

Molecular dipole moment scales linearly with density. This could be understood from simple argument.

The second contribution can be treated in mean-field approximation. By the chain rule for differentiation,

$$\frac{\partial|\bar{\mu}|}{\partial\rho} = \frac{\partial|\bar{\mu}|}{\partial E_l}\frac{\partial E_l}{\partial R}\frac{\partial R}{\partial\rho}. \tag{1}$$

Here, E_l is the projection of the local Coulomb field on the molecule along the $\angle$HOH bisector, and R is a measure of average molecular separation. The first factor on the RHS of (1) is the molecular polarizability α along the field direction, to leading order. Defining the density as $\rho = mR^{-3}$ we have $\partial R/\partial\rho \sim -R^4/m$. For the local field dependence on R, we assume leading term should be due to the permanent dipole μ_0, the separation R and an orientational factor $f(\theta)$ according to $\mu_0 f(\theta)/R^3$. Therefore

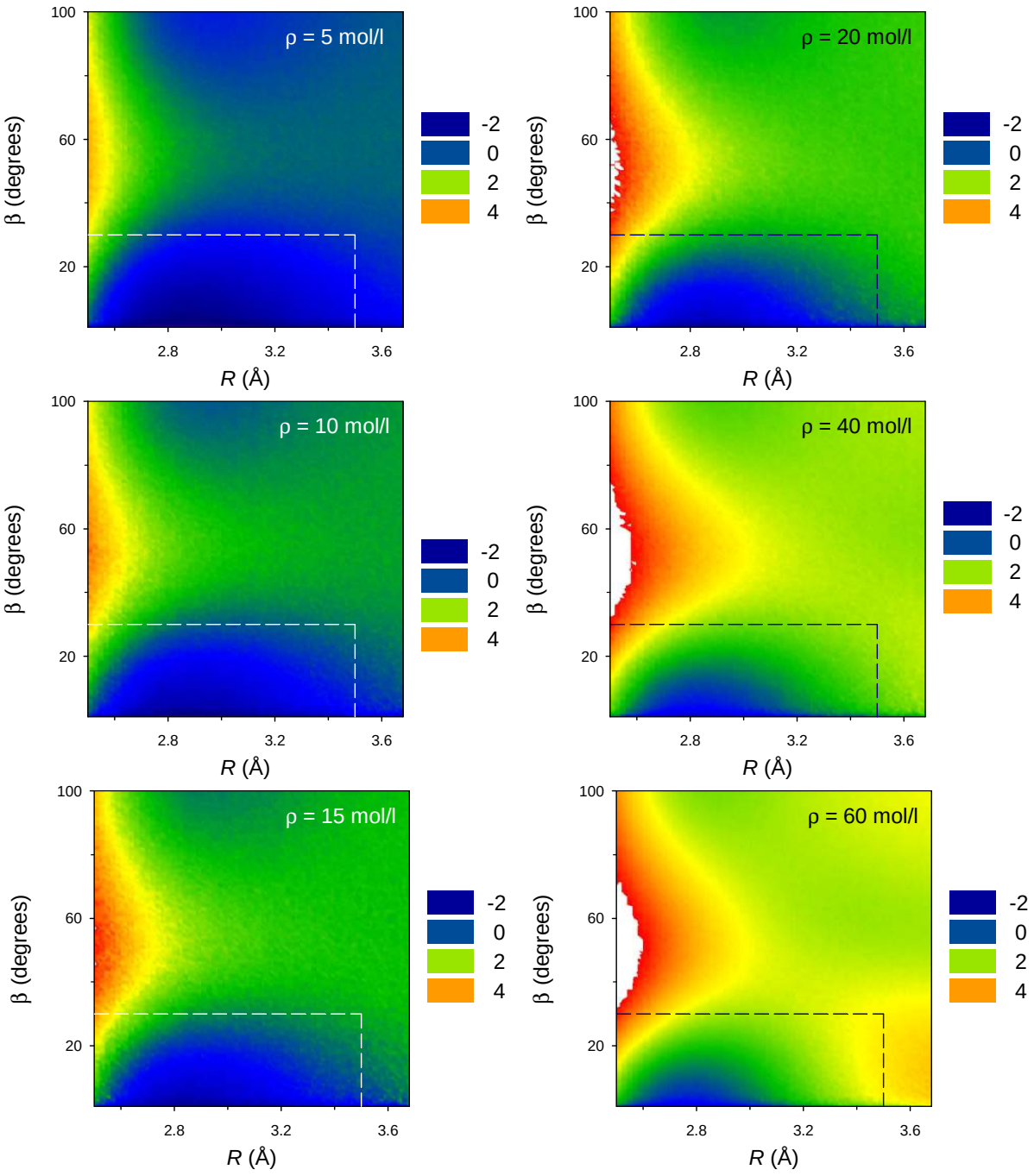

FIG. 3: Potential of mean force (in kT units) map in O–O and $\angle$OH$\cdots$O dimensions at various densities along the 673 K isotherm. The dashed lines of contrast colors fence the area of hydrogen-bonded molecules using our criterion.

$(\partial E/\partial R) \sim -\mu_0 f(\theta)/R^4$ and, finally, $\partial\mu/\partial\rho \sim \alpha\,\mu_0 f(\theta)/m$. Consequently, we expect the molecular dipole to depend approximately linearly on density with the observed change of slope indicative of an increase in local density as the HB network coalesces. This is consistent with the density dependence of the Onsager reaction field [9].

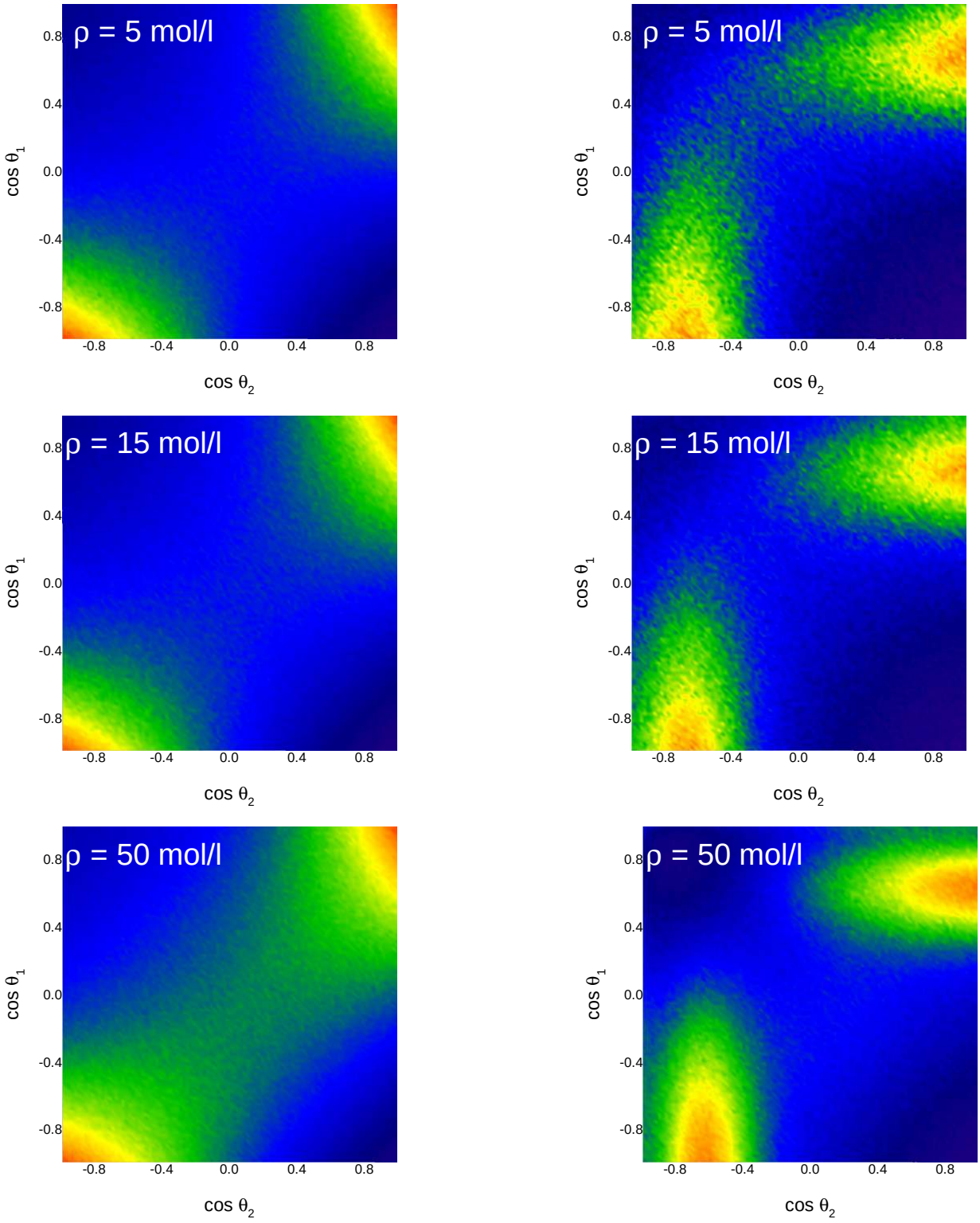

FIG. 4: Dipole moment correlation function for the first solvation shell for the Stockmayer fluid, left column; QDO water, right column at $T^* = 1.036 T_c$ at denoted densities.

Polarizable Stockmayer model

The original Stockmayer model, consisting of the Lennard-Jones (LJ) isotropic part and embedded point dipole, provides one of the simplest models for polar liquids. In particular, we study a dipole polarizable version using the parameters of Ref. [10] as a baseline. In order to run the simulations in the NAMD code [11], we replaced the point dipole by a pair of $\pm 0.52|e|$ point charges 0.6 Å apart, giving the permanent dipole moment of 1.5 D. A classical Drude model embedded to generate induction in the dipole limit. The oscillator consists of a point charge of $-0.5|e|$ harmonically tethered to the midpoint between the charges forming the fixed dipole; the latter bears a neutralizing charge of $+0.5|e|$. The generally accepted value for the water polarizability, $\alpha = 1.444\,\text{Å}^3$, defines the classical Drude spring constant, $k = 240\,\text{kJ mol}^{-1}\,\text{Å}^{-2}$. Apart from the Lennard-Jones terms between the Drude tether sites, with parameters $\epsilon = 3.1785$ kJ/mol and $\sigma = 2.955$ Å, a regularising LJ repulsion is added between the oscillators with parameters $\epsilon = 0.36854$ kJ/mol, $\sigma = 2.955$ Å.

Association topology

In order to study the short-range orientational correlations of water and the Stockmayer fluid, we calculated the probability distrinution function for two angles θ_i $i \in \{1, 2\}$ between molecular dipole moments and the vector connecting their COMs for the molecules in the first solvation shell (as defined by the 1st minima in $g_{\text{OO}}(r)$ radial distribution functions). The results presented in Fig. 4 show that while water prefers tetrahedral coordination, the Stockmayer fluid adopts a linear association topology.

[1] A. Jones, F. Cipcigan, V. P. Sokhan, J. Crain, and G. J. Martyna, Phys. Rev. Lett. **110**, 227801 (2013).
[2] A. Jones, A. Thompson, J. Crain, M. H. Muser, and G. J. Martyna, Phys. Rev. B **79**, 144119 (2009).
[3] A. P. Jones, J. Crain, V. P. Sokhan, T. W. Whitfield, and G. J. Martyna, Phys. Rev. B **87**, 144103 (2013).
[4] G. J. Martyna, M. E. Tuckerman, D. J. Tobias, and M. L. Klein, Mol. Phys. **87**, 1117 (1996).
[5] T. W. Whitfield and G. J. Martyna, J. Chem. Phys. **126**, 074104 (2007).
[6] A. Jones, J. Crain, F. Cipcigan, V. Sokhan, M. Modani, and G. Martyna, Mol. Phys. **111**, 3465 (2013).
[7] A. Jones and B. Leimkuhler, J. Chem. Phys. **135**, 084125 (2011).
[8] R. Kumar, J. R. Schmidt, and J. L. Skinner, J. Chem. Phys. **126**, 204107 (2007).
[9] L. Onsager, J. Am. Chem. Soc. **58**, 1486 (1936).
[10] M. van Leeuwen, Fluid Phase Equilibria **99**, 1 (1994).
[11] J. C. Phillips, R. Braun, W. Wang, J. Gumbart, E. Tajkhorshid, E. Villa, C. Chipot, R. D. Skeel, L. Kal, and K. Schulten, J. Comp. Chem. **26**, 1781 (2005).